Exp. Theo. NANOTECHNOLOGY 10 (2026) 277-287 https://doi.org/10.56053/10.S.277

Effect of changing magnetite percentage on structural and magnetic properties of cobalt ferrite prepared by the sol-gel method

Atheer. I. Abd Ali[1], *Mohammed RASHEED*[2,*]

[1] Applied Sciences Department, University of Technology- Iraq, Baghdad, Iraq
[2] Production Engineering & Metallurgy College, University of Technology- Iraq, Baghdad, Iraq
[*]) Email: rasheed.mohammed40@yahoo.com

Received 17/11/2025, *Received in revised form* 15/12/2025, *Accepted* 28/12/2025, *Published* 15/2/2026

The present research properly fabricated $Co_{1-x}Fe_2O_4$ nanoparticles (NPs) with a spinel structure (where x=0.3, 0.6, and 0.9, which corresponds to $Co_{0.4}Fe_2O_4$, $Co_{0.4}Fe_2O_4$, and $Co_{0.4}Fe_2O_4$) via a sol-gel approach with ferric nitrate, cobalt nitrate, and citric acid as precursors are used. The powders are compressed, sintered at 1000°C for 6 hours, then calcined at 500°C for 4 hours to produce dense pellets. X-ray diffraction revealed the production of a single-phase cubic spinel structure with a favored (311) orientation, and the crystallite size is determined to be between 40 and 80 nm. Vibrating sample magnetometry (VSM) demonstrated soft magnetic behavior with low coercivity and remanence, notably for the composition of $Co_{0.4}Fe_2O_4$ NPs. Microwave absorption characteristics determined with an X-band (8-12.5 GHz) network analyzer revealed that variations in Co content significantly affected density, porosity, and grain size, leading to changes in attenuation coefficient and scattering parameters (S11 and S21), with absorption following a Gaussian-type distribution. Furthermore, antibacterial activity as measured by the agar diffusion technique showed efficient suppression of *Escherichia coli* and *Staphylococcus aureus*, with greater activity versus the Gram-negative strain. These findings emphasize the multifunctionality of Co-doped cobalt ferrite nanomaterials.

Keywords: Cobalt ferrite; Sol-gel method; Ferromagnetic.

1. INTRODUCTION

Nanoparticle materials are one of the most widely studied objects with far-reaching implications in contemporary advances because they possess a variety of surface conditions. Owing to the ultra-small size of the particles, its magnetic properties may be enhanced [1-5]. Cobalt ferrite nanoparticles are one such material of importance for magnetic applications [6-10]. It is a known magnetic ceramic (CoFe2O4) that is used for the applications to microwaves and electric devices [11-13]. Cobalt ferrite can also serve as an electrocatalyst for oxygen evolution reaction (OER) [13,14] and the material applied to prepare electrodes to be used in electrochemical capacitors (or named supercapacitors) for energy storage [15, 16]. These applications utilize redox reactions on the surface of ferrite [16]. When controlled-size and shape cobalt ferrite and enhanced surface area (and hence a larger number of active sites) has been prepared, the properties of CoFe2O4 are extremely magnetic at room temperature [17, 20]. There are many techniques to synthesize cobalt ferrite such as microemulsion, sol-gel, chemical co-precipitation and hydrothermal methods, all of which are used in this study [21-26]. A conventional method for preparing cobalt ferrite nanoparticles is the sol-gel process [27]. In the present work Cobalt ferrite particles are fabricated by sol-gel method with varying pH and solution temperature during preparation to get nanoparticles having strong magnetic properties.

2. EXPERIMENTAL METHOD

The proportions of raw materials cobalt nitrate [$Co(NO_3)2.6H_2O$], ferric nitrate [$Fe(NO_3)3.9H_2O$], and citric acid [C6H8O7] are calculated based on their atomic/molecular weights. Considering the value of (X), three points, such as (0.9, 0.6, 0.3), are considered and doped to cobalt nitrate and ferric nitrate on a one-to-one stochiometric ratio with citric acid using different ratios of molar amounts. The mixture is agitated with 100 ml of distilled water in a glass beaker at sound and stirred over time by means of model LMS-1003 hot magnetic stirrers. While stirring, the pH of the solution is adjusted to (7) by drop-wise addition of ammonia solution. Heat the above solution on a hot plate at 60 °C for 30 min to form a homogeneous mixed solution, and after about three hours of continuous stirring, its temperature is raised to 80°C, during which time the sol-gel transformation is observed initially. For the loose gelatigenous structure of the gel, the latter is dried at 120 °C and further torch-burned until all gels are completely destroyed. The thin material is crushed into ferrite powder for a period of three minutes with an electric mill. Better crystallization and more homogeneous distribution of cations in the spinel crystals are obtained by calcining the burned ash at (500 °C) for 4 hours. The powders are mixed with glycerol having a 88% purity by weight in the proportion of 6%. The material is crushed at (100 MPa) by piston oil in order to make parallelogram-shaped samples with dimensions of (2.4 1.2-1.2 cm3).

3. SAMPLE CHARACTERIZATIONS

3.1 X-ray diffraction measurement

The structural properties are studied by conducting an X-ray diffraction (XRD) test utilizing Cu-Kα radiation with a wavelength of λ = 1.54060 Å [28]. The samples' Braggs angles are measured in the range of ($2\theta = 10 - 80^{o}$). The results showed a good agreement with Table Standard specifications (ASTM). The distance between the atomic levels (d) of the prepared samples is also calculated by applying the Braggs equation [29-35].

$$n\lambda = d \sin(\theta) \quad (1)$$

Scherer's formula is used to estimate the average crystal size (C.S.) [36-40]

$$C.S. = \frac{0.94\lambda}{\beta \cos(\theta)} \quad (2)$$

where β represents the full width half maximum (FWHM), λ refers to the XRD wavelength, while θ refers to the diffraction angle of XRD peak [15]. The porosity is also calculated using Eq. 5, after

calculating the theoretical density (ρ_{theo}) using Eq. 4 and bulk density (ρ_{bulk}) using Eq. 3 of the samples prepared [41-45]

$$\rho_{bulk} = \frac{m}{v} \quad (3)$$

$$\rho_{theo.} = \frac{8.M}{N_A.a^3} \quad (4)$$

$$P(\%) = \left(1 - \frac{\rho_{bulk.}}{\rho_{theo.}}\right) \quad (5)$$

where (M) represents the molecular mass, (N_A) is Avogadro's number, and (a) represents the lattice constant. The number 8 in Eq. 6 refers to the number of molecules in the unit cell [46, 47].

3.2 Measurement of electrical properties

The Reflection and Transmission coefficients are calculated using scattering parameters (S11, S21,),where S11 is (input reflection coefficient), S21 (forward transmission coefficient). S parameters are always measured in the form of decibel values (dB). To covert S parameters in the form of percentage (%), one must use the Eqns. 6 and 7 [47].

$$\text{Reflection Coefficient (R\%)} = 10^{(S11|_{dB}/_{10})} \quad (6)$$

$$\text{Transmission Coefficient (T\%)} = 10^{(S21|_{dB}/_{10})} \quad (7)$$

The absorbance % is done by substituting the result of Eqns.6 and 7 in Eq. 8 [9]

$$\text{Absorbance} = 1 - R^2 - T^2 \quad (8)$$

Calculating the attenuation coefficient or reflection loss in (dB) unit can be done using the following equation [7, 8].

$$\text{Attenuation Coefficient} = -20\ \text{Log}|S11| \quad (9)$$

3.3 Antibacterial activity

The antibacterial activity of $Co_{0.4}Fe_2O_4$ nanoparticles (NPs) is evaluated against the Gram-negative bacterium *Escherichia coli* (*E. coli*) and the Gram-positive bacterium *Staphylococcus aureus* (*S. aureus*) using the agar diffusion method (ADM). Sterile Mueller–Hinton agar plates are inoculated with bacterial suspensions adjusted to a 0.5 McFarland standard (approximately 1.5×10^8 CFU/mL). Wells with a diameter of 6 mm are aseptically prepared in the agar and filled with predetermined volumes of the $Co_{0.4}Fe_2O_4$ NPs suspensions. The plates are incubated at 37 °C for 24 h, after which the antibacterial efficacy is assessed by measuring the diameters of the inhibition zones surrounding each well. For this study, circular nanoparticle samples of $Co_{0.4}Fe_2O_4$ sintered at 1000 °C are employed.

3. RESULTS AND DISCUSSIONS

4.1 X-ray diffraction measurement results

Figure 1 displays the X-ray diffraction patterns of cobalt ferrite with formula $Co_{0.4}Fe_2O_4$. These Results indicated that all prepared samples have a polycrystalline structure and match perfectly with (ASTM) for $Co_{1-x}Fe_2O_4$ crystals. The diffraction pattern shows that the 2θ principal angles are (30.25°, 35.50°, 43.20°, 57.05°, and 62.85°) and belonging to diffraction levels (220), (311), (400), (511), and (440) as Millar indices. The sample $Co_{0.4}Fe_2O_4$ is the best sample because it had the lowest amount of porosity, While the other angles can be found in Table 1 correspondingly. The diffraction pattern reveals the samples' nanoparticle composition and cubic spinel structure development [59, 60]. There is no peak that corresponded to either materials or unusual phases. The Average crystal size and porosity are calculated as shown in Table 1. The molar ratio of cobalt to ferrite did not change significantly in the positions of the peaks as shown in Figure 2.

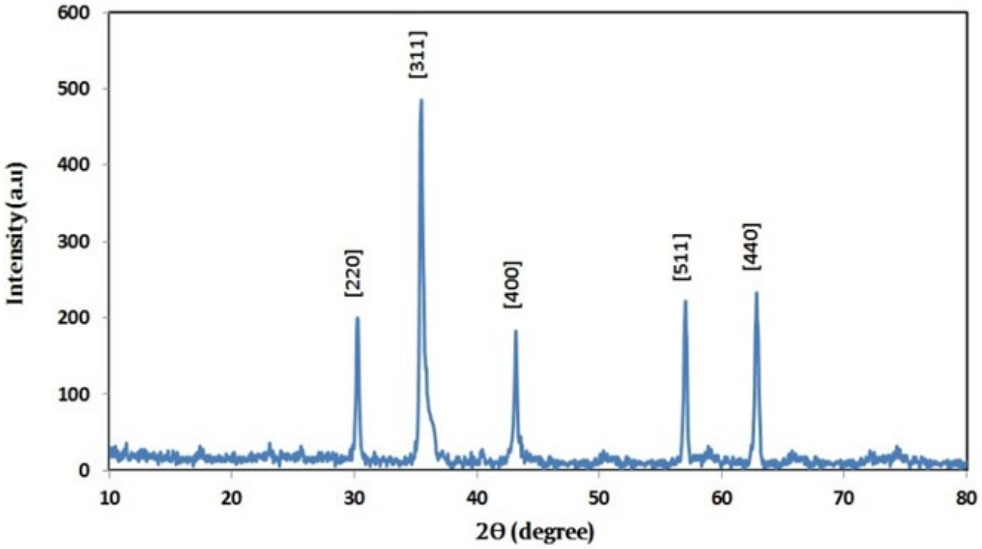

Figure 1 X-ray pattern of $Co_{0.4}Fe_2O_4$ samples.

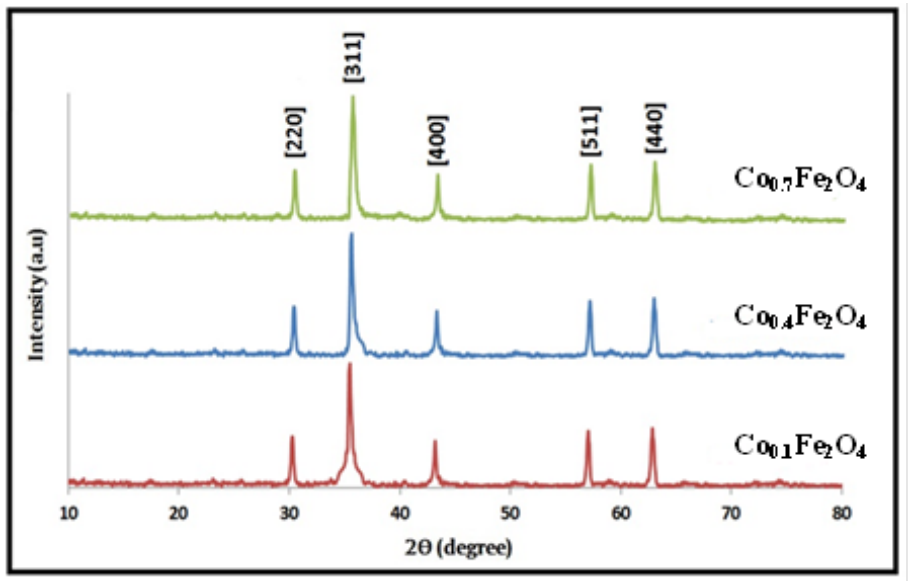

Figure 2 X-ray pattern of all samples with different molar ratio.

Table 1 The results of structural properties.

Samples	(hkl)	2θ° -XRD	D (nm)
	(220)	30.20	41.71
	(311)	35.45	44.25
$Co_{0.1}Fe_2O_4$	(400)	43.25	49.48
	(511)	57.1	66.33
	(440)	62.80	78.79
	(220)	30.25	41.73
	(311)	35.50	44.28
$Co_{0.4}Fe_2O_4$	(400)	43.20	49.44
	(511)	57.05	66.24
	(440)	62.85	78.93
	(220)	30.20	41.71
	(311)	35.55	44.31
$Co_{0.7}Fe_2O_4$	(400)	43.25	49.48
	(511)	57.05	66.24
	(440)	62.80	78.79

4.2 Electromagnetic properties measurements results

Figure 3 (a-d) shows the extremely high absorption values, particularly at the molar ratio ($Co_{0.4}Fe_2O_4$), with a good bandwidth at this molar ratio of 1.89 GHz for the frequency range (8.15-10.04 GHz) in the X-band region. The average absorptivity values across the entire X-band region are generally very high (91.95%), and these matters are similar to the sample ($Co_{0.1}Fe_2O_4$) but at a slower rate. The absorbance values for the sample ($Co_{0.7}Fe_2O_4$) clearly fluctuate, especially at frequencies of 8.29,10.11,11.55 GHz. Additionally, a material with a high absorbance value can be used in a variety of industries, particularly the military where it can be used to effectively conceal air targets from radar. The attenuation coefficient is shown in Figure 3, and it is clear that the best values are the molar ratios ($Co_{0.4}Fe_2O_4$) because they result in a reduction in porosity and an increase in density [14, 46]. The values of attenuation coefficient and absorbance are very high, particularly at the molar ratio ($Co_{0.4}Fe_2O_4$) with good bandwidth at this ratio for the entire X range. Because the ferric percentage has decreased, the molar ratio ($Co_{0.7}Fe_2O_4$) is fluctuating. The effect of cobalt doping ferrite results in a difference in composition and influences density, porosity, and particle size [33, 34]. This effect has a Gaussian distribution and changes the values of the attenuation and absorption coefficient due to the change in the dispersion coefficients (S11 and S21).

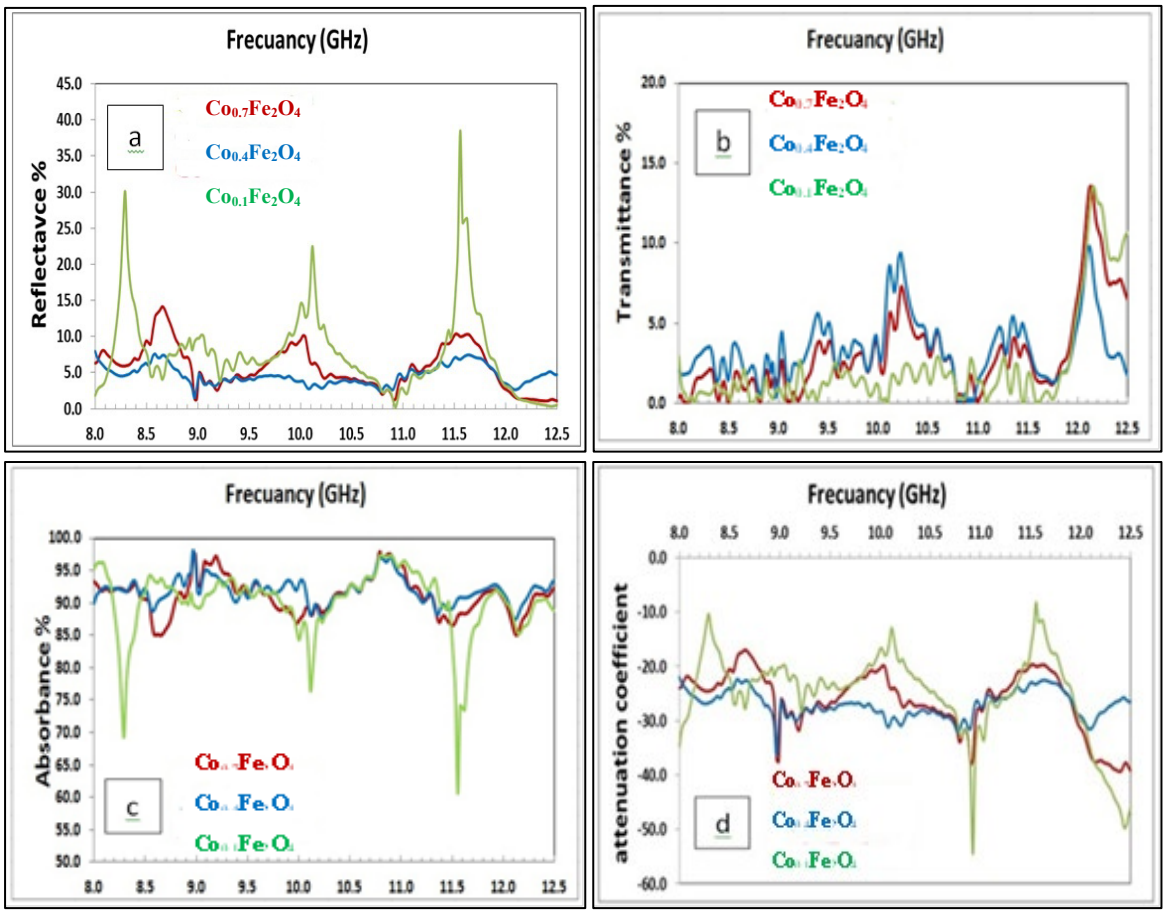

Figure 3 (a) the reflectance, (b) the transmittance, (c) the absorption, and (d) the attenuation coefficient, with the frequency at different molar ratio

4.3 VSM

Figure 4 illustrates the magnetic hysteresis loop obtained from Vibrating Sample Magnetometer (VSM) measurements for $Co_{0.4}Fe_2O_4$ (NPs) at room temperature, showing the variation of magnetization (emu/g) as a function of the applied magnetic field (B). The magnetization increases with the applied field and reaches an approximate saturation magnetization (Ms) of about 0.016–0.017 emu/g at the maximum applied field of ±15,000 G.

The M–H curve exhibits a narrow, S-shaped hysteresis loop with a very small coercive field (Hc), estimated to be on the order of a few hundred gauss or less, and a low remanent magnetization (Mr) of approximately 0.002–0.003 emu/g. This magnetic property implies that the $Co_{0.4}Fe_2O_4$ (NPs) have soft magnetic properties with a trend to superparamagnetic or mild ferromagnetic activity, as is common of ferrite nanoparticles in the 40-80 nm size range. The low coercivity may be due to the tiny particle size, which inhibits domain wall motion and promotes single-domain or near-superparamagnetic states. The quick rise in magnetization at low magnetic fields shows the ease with which magnetic moments align, but the slow progression toward saturation at higher fields indicates the existence of surface-related magnetic influences. Even at the maximum applied field, complete saturation is not entirely attained, as is typically found in nanoscale ferrites, owing to surface spin disorder and spin canting caused by broken exchange bonds and decreased coordination of surface atoms [6]. The relatively low saturation magnetization compared to bulk cobalt ferrite is mainly attributed to cation redistribution between tetrahedral (A) and octahedral (B) sites in the spinel lattice, partial substitution of Co ions,

and the increased surface-to-volume ratio at the nanoscale. The presence of Co^{2+} ions at octahedral sites contributes to magneto-crystalline anisotropy, while Fe–O–Fe super-exchange interactions dominate the overall magnetic response. The VSM results confirm that $Co_{0.4}Fe_2O_4$ (NPs) exhibit low coercivity, low remanence, and moderate saturation magnetization, making them suitable for applications requiring soft magnetic behavior and low hysteresis losses, such as microwave absorption, electromagnetic interference (EMI) shielding, and certain biomedical applications [5].

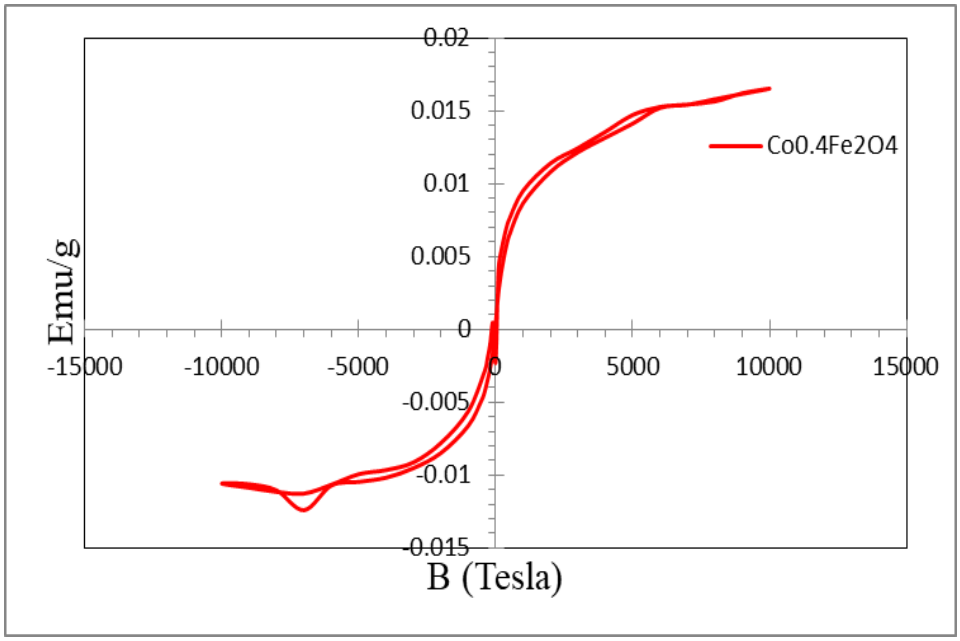

Figure 4 VSM hysteresis loop of $Co_{0.4}Fe_2O_4$ (NPs) measured at room temperature, showing a narrow S-shaped M–H curve with low coercivity and remanence, indicative of soft magnetic behavior and an approach to saturation at higher applied fields

4.4 Antibacterial activity

Figure 5 shows the antibacterial activity of $Co_{0.4}Fe_2O_4$ (NPs) against Gram-negative Escherichia coli (*E. coli*) and Gram-positive *Staphylococcus aureus* (*S. aureus*) as measured by the agar diffusion technique (ADM). The antibacterial efficiency is measured by measuring the width of the inhibition zone (ZOI) produced around the nanoparticle-loaded well after 24 hours of incubation at 37 degrees Celsius. The $Co_{0.4}Fe_2O_4$ (NPs) showed a strong inhibitory impact against both bacterial strains, demonstrating their antibacterial properties. *E. coli* had a wider inhibitory zone of 12.74 mm, whereas *S. aureus* had a smaller zone of 9.72 mm. This disparity suggests that nanoparticles are more efficient against Gram-negative bacteria than Gram-positive bacteria [40]. The increased antibacterial action against *E. coli* is due to structural changes in the bacterial cell walls. Gram-negative bacteria have a smaller peptidoglycan layer and an outer membrane containing lipopolysaccharides, which may allow for stronger interactions with nanoparticles and increase penetration or membrane breakdown. In comparison, *S. aureus*, a Gram-positive bacterium, has a thicker peptidoglycan layer that functions as a protective barrier, lowering sensitivity to nanoparticle-induced damage.

The antibacterial process of $Co_{0.4}Fe_2O_4$ (NPs) is most likely due to a variety of factors, including the generation of reactive oxygen species (ROS), electrostatic interactions between positively charged NPs surfaces and negatively energized bacterial membranes, and the potential release of metal ions that interfere with cellular metabolic processes. Furthermore, the nanoscale size and large surface area of the particles improve interaction with bacterial cells, enhancing antibacterial efficacy. The findings

show that $Co_{0.4}Fe_2O_4$ (NPs) have broad-spectrum antibacterial action, with higher inhibition versus *E. coli* than *S. aureus*. This selected yet effective antibacterial activity emphasizes their potential use in antimicrobial coatings, biomedical materials, and environmental remediation technologies [42].

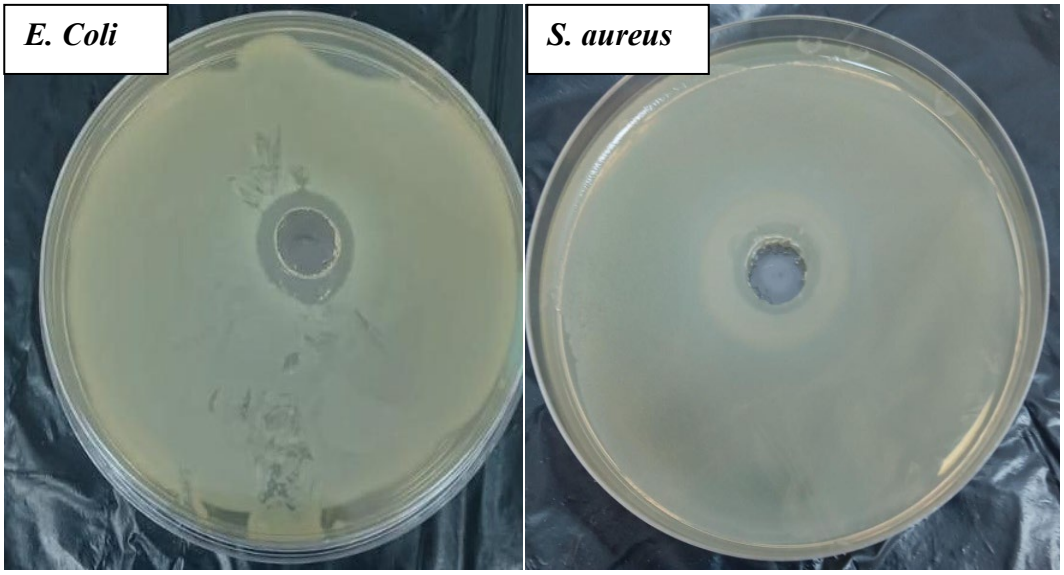

Figure 5. Antibacterial action of $Co_{0.4}Fe_2O_4$ (NPs) determined via the agar diffusion technique (ADM) against (a) *E. coli* and (b) *S. aureus* after 24 hrs of incubation at 37°C.

5. CONCLUSIONS

Cobalt ferrite nanoparticles with specified compositions are effectively produced by the sol-gel process, indicating that the molar ratio plays a critical role in customizing the structural, magnetic, microwave, and antibacterial characteristics of $Co_{1-x}Fe_2O_4$ NP ferrites. X-ray diffraction indicated that all samples crystallized in a single-phase cubic spinel structure, with a favored (311) orientation and nanoscale crystallite sizes ranging from 40 to 80 nm. Among the examined compositions, $Co_{0.4}Fe_2O_4$ (NPs) demonstrated the most advantageous microstructural features, including decreased porosity and increased densification, which favorably affected its functional performance. Vibrating sample magnetometry (VSM) revealed that $Co_{0.4}Fe_2O_4$ (NPs) possess soft magnetic behavior, characterized by a low coercive field ($Hc \approx$ a few hundred gauss), low remanent magnetization ($Mr \approx$ 0.002-0.003 emu/g), and moderate saturation magnetization ($Ms \approx$ 0.016-0.017 emu/g). This magnetic response was due to nanoscale particle size, surface spin disorder, and cation redistribution within the spinel lattice, making the material appropriate for applications with minimal hysteresis losses. Antibacterial activity was assessed using the agar diffusion technique, and $Co_{0.4}Fe_2O_4$ (NPs) inhibited both Gram-negative and Gram-positive bacteria. The observed zones of inhibition for *Escherichia coli* and *Staphylococcus aureus* were 12.74 mm and 9.72 mm, respectively, demonstrating higher antibacterial activity against the Gram-negative strain due to variations in cell wall structure. The results confirm that a non-random molar ratio—especially $Co_{0.4}Fe_2O_4$ (NPs)—is essential for achieving cobalt ferrite nanoparticles with optimized magnetic, microwave absorption, and antibacterial properties, highlighting their potential for electromagnetic interference shielding, microwave absorption, and antimicrobial applications.

REFERENCES

[1] M. Sajjia, M. Oubaha, M. Hasanuzzaman, A. G. Olabi. Ceram. Int. 40 (2014) 1147 https://doi.org/10.1016/j.ceramint.2013.06.116

[2] M. M. El-Okr, M. A. Salem, M. S. Salim, R. M. El-Okr, M. Ashoush, H. M. Talaat. J. Magn. Magn. Mater. 323 (2011) 920 https://doi.org/10.1016/j.jmmm.2010.11.069
[3] A. Hannour, D. Vincent, F. Kahlouche, A. Tchangoulian, S. Neveu, V. Dupuis. J. Magn. Magn. Mater. 353 (2014) 29 https://doi.org/10.1016/j.jmmm.2013.10.010
[4] J.-G. Lee, J. Y. Park, and C. S. Kim, "Growth of ultra-fine cobalt ferrite particles by a sol–gel method and their magnetic properties," J. Mater. Sci. 33 (1998) 3965 https://doi.org/10.1023/a:1004696729673
[5] N. A. Al-Rubaiey, F. S. Kadhim, A. A. Ati, Eng. Tech. J. 35 (2017) 849 https://doi.org/10.30684/etj.35.8a.11
[6] Dipti Biswal, B. N. Peeples, C. Peeples, A. K. Pradhan. J. Magn. Magn. Mater. 345 (2013) 1 https://doi.org/10.1016/j.jmmm.2013.05.052
[7] R. M. Mohamed, M. M. Rashad, F.A. Haraz, and W. M. Sigmund, J. Magn. Magn. Mater, 322 (2010) 2058 https://doi.org/10.1016/j.jmmm.2010.01.034
[8] S. O. Estrada, C. A. Huerta-Aguilar, T. Pandiyan, M. Corea, I. A. Reyes-Domínguez, G. Tavizon, J. Alloys Compd. 695 (2017) 2706 https://doi.org/10.1016/j.jallcom.2016.11.187
[9] N. Moumen, P. Veillet, M. P. Pileni, J. Magn. Magn. Mater. 149 (1995) 67 https://doi.org/10.1016/0304-8853(95)00340-1
[10] I. Alshalal, H. M. I. Al-Zuhairi, A. A. Abtan, M. Rasheed, M. K. Asmail. J. Mech. Behav. Mater. 32 (2023) 1 https://doi.org/10.1515/jmbm-2022-0280
[11] M. Sellam, M. Rasheed, S. Azizi, T. Saidani. Ceram. Int. 50 (2024) 20917 https://doi.org/10.1016/j.ceramint.2024.03.094
[12] O. Alabdali, S. Shihab, M. Rasheed, T. Rashid. 3rd inter. Scient. conf. alkafeel univ. (ISCKU 2021) (2022) https://doi.org/10.1063/5.0066860
[13] M. Rasheed, O. Alabdali, S. Shihab, A. Rashid, T. Rashid, J. Phys.: Conf. Ser. 1999 (2021) 012078 https://doi.org/10.1088/1742-6596/1999/1/012078
[14] N. Assoudi et al. Opt. Quant. Electron. 54 (2022) 9 https://doi.org/10.1007/s11082-022-03927-x
[15] R. Jalal, S. Shihab, M.A. Alhadi, M. Rasheed, J. Phys.: Conf. Ser. 1660 (2020) 012090 https://doi.org/10.1088/1742-6596/1660/1/012090
[16] S. Shihab, M. Rasheed, O. Alabdali, A.A. Abdulrahman, J. Phys.: Conf. Ser. 1879 (2021) 022120 https://doi.org/10.1088/1742-6596/1879/2/022120
[17] A. Keziz, M. Heraiz, M. RASHEED, A. Oueslati. Mater Chem. Phys. 325 (2024) 129757 https://doi.org/10.1016/j.matchemphys.2024.129757
[18] D. Kherifi, A. Keziz, M. Rasheed, A. Oueslati. Ceram. Int. 50 (2024) 30175 https://doi.org/10.1016/j.ceramint.2024.05.317
[19] A. Jaber, M. Ismael, T. Rashid, M. A. Sarhan, M. Rasheed, I. M. Sala. Eureka: Phys. Eng. 4 (2023) 29 https://doi.org/10.21303/2461-4262.2023.002770
[20] T. Rashid, M. M. Mokji, M. Rasheed. J. Optics 18 (2024) 99 https://doi.org/10.1007/s12596-024-02080-w
[21] H. K. Aity, E. Dhahri, M. Rasheed. Ceram. Int. 50 (2024) 54666 https://doi.org/10.1016/j.ceramint.2024.10.324
[22] M. Rasheed, S. Shihab, O. Alabdali, A. Rashid, T. Rashid, J. Phys.: Conf. Ser. 1999 (2021) 012077 https://doi.org/10.1088/1742-6596/1999/1/012077
[23] M. Rasheed, M. Nuhad Al-Darraji, S. Shihab, A. Rashid, T. Rashid. J. Phys.: Conf. Ser. 1963 (2021) 012058 https://doi.org/10.1088/1742-6596/1963/1/012058
[24] A. Keziz, M. Heraiz, F. Sahnoune, M. Rasheed, Ceram. Int. 49 (2023) 32989 https://doi.org/10.1016/j.ceramint.2023.07.275
[25] E. Kadri, K. Dhahri, R. Barillé, M. Rasheed. Phase Transitions 94 (2021) 65 https://doi.org/10.1080/01411594.2020.1832224
[26] D. Bouras, M. Rasheed, Opt. Quantum Electron. 54 (2022) 12 https://doi.org/10.1007/s11082-022-04161-1

[27] A. Zubaidi, L.M. Asaad, I. Alshalal, M. Rasheed, J. Mech. Behav. Mater. 32 (2023) 1 https://doi.org/10.1515/jmbm-2022-0302
[28] M. Rasheed et al., J. Phys.: Conf. Ser. 1999 (2021) 012080 https://doi.org/10.1088/1742-6596/1999/1/012080
[29] M. Rasheed, M.N. Al-Darraji, S. Shihab, A. Rashid, T. Rashid, J. Phys.: Conf. Ser. 1963 (2021) 012059 https://doi.org/10.1088/1742-6596/1963/1/012059
[30] M. Enneffatia, M. Rasheed, B. Louati, K. Guidara, S. Shihab, R. Barillé, J. Phys.: Conf. Ser. 1795 (2021) 012050 https://doi.org/10.1088/1742-6596/1795/1/012050
[31] M. Rasheed, O.Y. Mohammed, S. Shihab, A. Al-Adili, J. Phys.: Conf. Ser. 1795 (2021) 012043 https://doi.org/10.1088/1742-6596/1795/1/012043
[32] A.H. Ali, A.S. Jaber, M.T. Yaseen, M. Rasheed, O. Bazighifan, T.A. Nofal, Complexity 2022 (2022) 1 https://doi.org/10.1155/2022/9367638
[33] M. Rasheed, et al., J. Adv. Biotechnol. Exp. Ther. 6 (2023) 495 https://doi.org/10.5455/jabet.2023.d144
[34] M. Rasheed, I. Alshalal, A.A. Ashed, M.A. Sarhan, A.S. Jaber, Indones. J. Electr. Eng. Comput. Sci. 33 (2024) 653 https://doi.org/10.11591/ijeecs.v33.i1.pp653-660
[35] I.M. Mohammed, M. Rasheed, AIP Conf. Proc. 3321 (2025) 020026 https://doi.org/10.1063/5.0289719
[36] F. Boudou, A. Belakredar, A. Berkane, M. Rasheed, Not. Sci. Biol. 17 (2025) 12183 https://doi.org/10.55779/nsb17212183
[37] F. Boudou, et al., Not. Sci. Biol. 17 (2025) 12593 https://doi.org/10.55779/nsb17312593
[38] F. Boudou, A. Guendouzi, A. Belkredar, M. Rasheed, Not. Sci. Biol. 16 (2024) 13837 https://doi.org/10.55779/nsb16211837
[39] R.S. Mahmood, et al., J. Mech. Behav. Mater. 34 (2025) 1 https://doi.org/10.1515/jmbm-2025-0040
[40] T. Rashid, M.M. Mokji, M. Rasheed, J. Mech. Behav. Mater. 34 (2025) 77 https://doi.org/10.1515/jmbm-2025-0074
[41] M. Rasheed, M. N. Mohammedali, F. A. Sadiq, M. A. Sarhan, T. Saidani. J. Optics (New Delhi. Print) (2024) https://doi.org/10.1007/s12596-024-01928-5
[42] A.J. Hussein, M.N. Al-Darraji, M. Rasheed, M.A. Sarhan, IOP Conf. Ser.: Earth Environ. Sci. 1262 (2023) 022007 https://doi.org/ 10.1088/1755-1315/1262/2/022007
[43] A.J. Hussein, M.N. Al-Darraji, M. Rasheed, M.A. Sarhan, IOP Conf. Ser.: Earth Environ. Sci. 1262 (2023) 022005 https://doi.org/10.1088/1755-1315/1262/2/022005
[44] T. Saidani, M. Rasheed, I. Alshalal, A.A. Rashed, M.A. Sarhan, R. Barillé, Res. Eng. Struct. Mater. 10 (2) (2024) 743 http://dx.doi.org/10.17515/resm2023.21ma0922rs
[45] A. M. Shehap, Kh.H. Mahmoud, M.F.H. Abdelkader, Tarek M. El-Basheer, Experimental and Theoretical NANOTECHNOLOGY 1 (2017) 103 https://doi.org/10.56053/1.2.103
[46] Badis Bendjemil, Mahiedinne Ali-Rachedi, Jamal Bougdira, Faming Zhang, Eberhard Burkel, Experimental and Theoretical NANOTECHNOLOGY 1 (2017) 145 https://doi.org/10.56053/1.3.145
[47] L.A. Carrero Bermúdez, R. Moreno Mendoza, R. Cardona, D.A. Landínez Téllez, J. Roa-Rojas, Experimental and Theoretical NANOTECHNOLOGY 1 (2017) 161 https://doi.org/10.56053/1.3.161